Upscaling soil-atmosphere CO_2 and CH_4 fluxes across a topographically complex forested landscape

Authors:

Daniel L. Warner[1], Mario Guevara[1], Shreeram Inamdar[1], and Rodrigo Vargas[1*]

Affiliations:

[1]University of Delaware Department of Plant and Soil Sciences, Newark, Delaware, USA

*Corresponding Author

Rodrigo Vargas

University of Delaware

146 Townsend Hall

Newark, DE 19716

rvargas@udel.edu

(302) 831-1388

Highlights

- Soil flux predictions closely matched observations across seasons
- We used a machine learning approach to upscale soil fluxes and estimate uncertainty
- Temperature was positively related to CO_2 efflux and CH_4 uptake
- CH_4 fluxes had bi-directional responses to seasonal precipitation patterns

Abstract

Upscaling soil-atmosphere greenhouse gas (GHG) fluxes across complex landscapes is a major challenge for environmental scientists and land managers. This study employs a quantile-based digital soil mapping approach for estimating the spatially continuous distributions (2 m spatial resolution) and uncertainties of seasonal mean mid-day soil CO_2 and CH_4 fluxes. This framework was parameterized using manual chamber measurements collected over two years within a temperate forested headwater watershed. Model accuracy was highest for early (r^2 = 0.61) and late summer (r^2 = 0.64) for CO_2 and CH_4 fluxes. Model uncertainty was generally lower for predicted CO_2 fluxes than CH_4 fluxes. Within the study area, predicted seasonal mean CO_2 fluxes ranged from 0.17 to 0.58 μmol m^{-2} s^{-1} in winter, and 1.4 to 5.1 μmol m^{-2} s^{-1} in early summer. Predicted CH_4 fluxes across the study area ranged from -0.52 to 0.02 nmol m^{-2} s^{-1} in winter, and -2.1 to 0.61 nmol m^{-2} s^{-1} in early and late summer. The models estimated a per hectare net GHG potential ranging from 0.44 to 4.7 kg CO_2 eq. hr^{-1} in winter and early summer, with an estimated 0.4 to 1.5% of emissions offset by CH_4 uptake. Flux predictions fell within ranges reported in other temperate forest systems. Soil CO_2 fluxes were more sensitive to seasonal temperature changes than CH_4 fluxes, with significant temperature relationships for soil CO_2 emissions and CH_4 uptake in pixels with high slope angles. In contrast, soil CH_4 fluxes from flat low-lying areas near the stream network within the watershed were significantly correlated to seasonal precipitation. This study identified key challenges for modeling high spatial resolution soil CO_2 and CH_4 fluxes, and suggests a larger spatial heterogeneity and complexity of underlying processes that govern CH_4 fluxes.

Keywords: carbon dioxide, methane, hot-moments, hot-spots, digital soil mapping, topography, machine learning

1. Introduction

The increase in atmospheric concentrations of greenhouse gases (GHG) such as CO_2 and CH_4 has major implications for the health of humans and ecological systems worldwide. Although human activities largely contribute to the increases in GHG concentrations, natural sources and sinks of both CO_2 and CH_4 account for large portions of their respective budgets from local to global scales (King et al., 2015; Le Quéré et al., 2018; Saunois et al., 2016). Soils are a major source of CO_2 and may act as both a major source or sink of CH_4. Soil CO_2 efflux represents the largest fraction of total terrestrial CO_2 emissions (Raich and Potter, 1995). Anoxic saturated soils such as those found in wetland environments are estimated to represent roughly 20-30% of global CH_4 emissions, while well-drained upland soils account for roughly 5-10% of the CH_4 removed from the atmosphere annually (Dlugokencky et al., 2011).

Temperate forests are a major ecosystem type at the global scale, covering much of the eastern United States, Central and Eastern Europe, and East Asia (Friedl et al., 2002). These ecosystems store large quantities of carbon in their vegetation biomass and soils (Pan et al., 2011; Post et al., 1982), and these ecosystem components exchange large quantities of carbon with the atmosphere in the form of CO_2 and CH_4 (Gough et al., 2007; Warner et al., 2017). Soil-atmosphere CO_2 and CH_4 fluxes in temperate forests are highly heterogeneous in space, varying across regional scales with climate, ecoregion, and land use types (Ambus and Christensen, 1995; Raich and Tufekcioglu, 2000; Smith et al., 2000); and at landscape scales with vegetation cover, hydrologic conditions, and topographic heterogeneity (Atkins et al., 2014; Gomez et al., 2017; Maier et al., 2017; Reyes et al., 2017; Warner et al., 2018). Fluxes also vary temporally with diel patterns in temperature and plant activity, and with seasonally changing patterns in temperature, precipitation, and plant phenology (Crill, 1991; Phillips et al., 2010; Vargas and

Allen, 2008; Wang et al., 2013). Thus, the spatiotemporal heterogeneity of soil-atmosphere CO_2 and CH_4 fluxes is especially large in topographically complex landscapes that experience seasonal climates, and accurately quantifying CO_2 and CH_4 fluxes in these ecosystems is a major challenge for estimating and managing local to regional carbon budgets (King et al., 2015; Tonitto et al., 2016).

This scientific challenge has been approached in different ways. Top-down flux measurement techniques such as eddy covariance can measure fluxes at the ecosystem scale, but often are not well-suited for use in topographically heterogeneous terrain (Baldocchi, 2003; Baldocchi et al., 2000). Smaller scale techniques, such as flux chamber measurements employing portable gas analyzers, can better describe the heterogeneity of fluxes across different sources and sinks in an ecosystem (Gomez et al., 2017; Leon et al., 2014; Maier et al., 2017; Warner et al., 2017). However, upscaling manual chamber flux measurements to the ecosystem scale, and assessing relative importance of different sources and sinks within an ecosystem, is difficult because of their small measurement footprint (Phillips et al., 2017, Vargas et al., 2011). An alternative approach of landform classification and aggregation of mean fluxes from point measurements within each landform has been employed for estimating watershed scale soil-atmosphere CO_2 (Gomez et al., 2016; Riveros-Iregui and McGlynn, 2009; Webster et al., 2008a) and CH_4 fluxes (Gomez et al., 2016) in temperate ecosystems. However, studies incorporating topographic variability into ecosystem scale predictions of *in situ* chamber flux measurements of multiple GHGs are scarce. The aggregation of major landform elements, while useful, assumes spatial homogeneity of fluxes within each landform and does not reflect the spatially continuous nature of the land surface and soil processes at fine spatial resolutions. Furthermore, there is a lack of standardization in defining landforms, which hinders potential comparisons of findings across studies and across ecosystem types. A continuous approach to scaling point measurements across topographically complex landscapes could potentially address both of these issues by providing continuous, high resolution maps of fluxes describing the functional variability of soils within and across landform categories. In the context of this study and the previous studies mentioned above, topographic or terrain "complexity" and "variability" refer to medium scale topographic variations that are sufficiently described by a 2-meter resolution digital elevation model (DEM). This may include landscape features like convergent and divergent slopes, riparian zones, slope shoulders, and slope orientations, but excludes microtopographic variations that may be obscured at a 2-meter pixel size, such as small bumps and divots in the land surface.

The field of digital soil mapping has expanded with the rapid acceleration of computer processing, and has found many novel applications for soil scientists attempting to model the continuous spatial distributions of soil properties (McBratney et al., 2003). Digital soil mapping utilizes high-resolution DEMs, remote sensing data, legacy maps, and climate data to represent the soil forming environment and predict soil properties across landscapes where information is scarce. Machine learning or hypothesis driven models are used to couple field measurements of soil properties to spatial covariates derived from these publicly available data sources in order to generate predicted distributions of soil properties, classes, or functions (Hengl et al., 2017, 2004; McBratney et al., 2003; Wiesmeier et al., 2011). As soil-atmosphere GHG fluxes are ultimately a product of soil biogeochemical processes that are influenced by soil properties, we postulated that digital soil mapping is an alternative, low-cost approach to predict the magnitude and variability of soil CO_2 and CH_4 fluxes with high spatial resolution across a piedmont landscape.

Our overarching goals were to develop a framework for "upscaling" manual soil GHG chamber flux measurements to a continuous spatial distribution across complex terrain that could be employed in future and existing soil chamber flux studies, and examine how this continuous approach may reveal shifting spatial patterns of fluxes across seasons. In this study, we applied a digital soil mapping approach to upscale two years of existing flux measurements within a forested, northern piedmont watershed at seasonal scales. The goals of this study were to: 1) evaluate data-model agreement between chamber CO_2 and CH_4 flux measurements and terrain attributes using a digital soil mapping approach, 2) assess the spatial relationships between predicted soil CO_2 and CH_4 fluxes and seasonal changes in temperature and precipitation. We hypothesized that terrain attributes, including slope, aspect, and other terrain attributes, could be reliable predictors of soil CO_2 and CH_4 fluxes, given that other soil forming factors like vegetation and climate were relatively homogeneous in our spatial domain.

2. Methods

2.1 Study site and sampling design

This study was conducted in a 12-hectare forested headwater watershed at Fair Hill Natural Resources Management Area, Cecil County, Maryland, USA (39^{o} 42’ N, 75^{o} 50’ W). Forest vegetation is primarily composed of *Fagus grandifolia*, *Quercus spp.*, *Lirodendron tulipifera*, and *Acer spp* (Warner et al., 2017). Soils within the study area are coarse-loamy, mixed, mesic Lithic Dystrudepts belonging to the Manor and Glenelg series loams, which overlay pelitic gneiss and schist bedrock (Anderson and Matthews, 1973). Annual precipitation is approximately 1200 mm. Annual mean air temperature is 12 ^{o}C, reaching a maximum of 25 ^{o}C and minimum of -0.6 ^{o}C (DEOS 2017). The watershed has hilly topography typical of the Northern Piedmont, with a total elevation change of 31 m. Flux measurement locations had been distributed 20 sampling locations across four hillslope transects with sampling points that spanned valley bottoms, slopes, and upland areas as part of a study examining the influence of topography on soil properties and fluxes (Warner et al., 2018, Fig 1). A transect design was chosen for logistical reasons, as it maximized the number of measurements that could be taken within a mid-day window to avoid confounding diurnal effects (e.g., rapid changes in temperature and storm fronts) on fluxes (Cueva et al., 2017). Transects varied in length (27 to 70 m), elevation gain (6 to 14 m), and maximum slopes (9 to 25 percent).

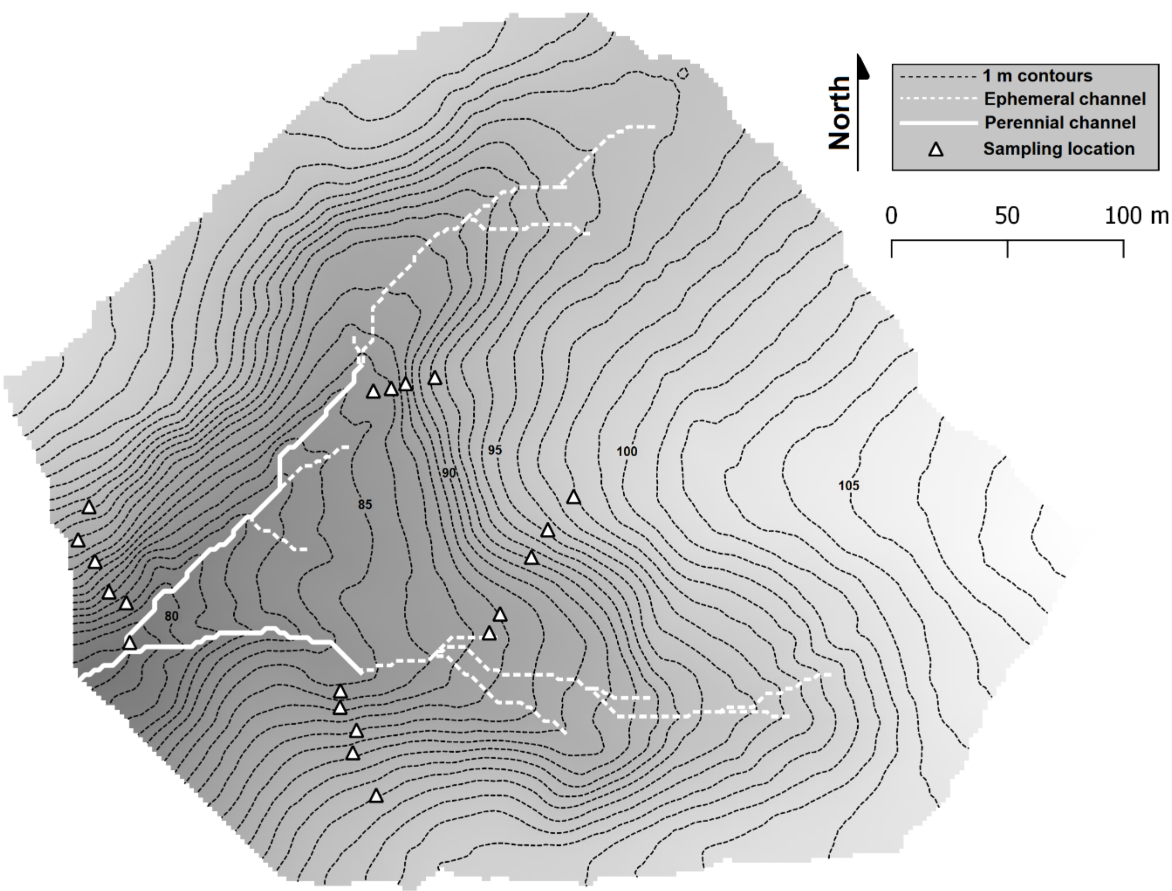

Figure 1. DEM and contour map of the study watershed. Sampling points are denoted by triangles, the perennial stream network is denoted by a solid white line, and ephemeral channels are denoted by white dashed lines.

2.2 Flux measurements

Soil-atmosphere CO_2 and CH_4 fluxes were measured from 10 cm diameter, 9 cm tall PVC collars inserted 5 cm into the soil at each sampling point along the transects. Fluxes were calculated based on the change of gas concentration within the chamber over the course of three minutes, which was measured with an ultraportable greenhouse gas analyzer (Los Gatos Research, Mountain View, California, USA) as described previously (Warner et al. 2017). Measurements were taken at mid-day (11:00 – 15:00) two times monthly from September 2014 to November 2016, with additional measurements following precipitation events and during drought periods, yielding a set of 880 total flux measurements. These measurements were classified by season based on annual patterns of soil temperature and moisture, which were measured from 0 to 4 cm with a handheld probe simultaneously with fluxes. Seasons were defined as winter (cold-wet: Jan 1-Feb 28), spring (warm-wet: Mar 1-May 20), early summer (hot-wet: May 20-Jul 31), late summer (hot-dry: Aug 1-Sep 30), and fall (warm-dry: Oct 1-Dec 31). Seasonal groupings were determined based on site-specific temperature, precipitation, and phenological patterns (Warner et al., 2018).

2.3 Topographic analysis and processing

Topographic data was acquired from a LiDAR (Light Detecting and Ranging)-derived DEM with 2 meter spatial resolution (NOAA, 2005). The DEM was preprocessed and conditioned for further topographic and hydrologic analysis (Jenson and Domingue, 1988). Flow direction was calculated as the maximum triangle slope (Tarboton, 1997). Primary and secondary terrain attributes were derived from this DEM in SAGA GIS (Conrad et al., 2015), and a full list of these attributes is provided in Supplementary Table 1. A GPS (Geographical Positioning System) survey was conducted to locate each chamber within 1-meter accuracy, allowing us to accurately identify the corresponding pixels on the terrain attribute grids.

2.4 Modeling fluxes and prediction uncertainty with quantile regression forests

Our digital soil mapping framework is summarized in Figure 2. Of the 27 topographic attributes considered, the attributes that were ultimately used in our predictions were selected for each season using the random forest-based variable selection method proposed by Genuer et al. (2012). A list of these variables and their descriptions is provided in Table 1, as is a comparison of summary statistics and distributions of each variable for the whole study watershed and for the set of sampling points where flux measurements were taken. This method uses a repeated cross validation procedure to select the most informative variables for model interpretation and model prediction purposes. The variables are first ranked by importance and eliminated systematically to reduce model error, ultimately yielding a small set of highly important variables that are sufficient for making robust predictions (Table 2).

This study employed quantile regression forests (Meinshausen, 2006), a variant of the random forests algorithm (Breiman, 2001). The random forests algorithm creates an ensemble of regression trees based on bagging, a statistical sub-setting technique applied to available data and available predictors. The final prediction is the average of all the regression trees which are evaluated by an out-of-bag cross-validation form. Alternatively, the quantile regression forests algorithm estimates the variance of all the ensembled trees (not just the mean as with the original random forests algorithm), producing a full conditional distribution of the response variable (i.e.,

Table 1. Selected variables used in quantile regression forests models. Summary statistics for each variable are provided for the whole study watershed and the sampling points. The third column provides D-statistics and p-values from Kolmogorov-Smirnoff Tests comparing the distributions of variables for the whole watershed and set of sampling points.

ID Number	Attribute	Summary (Watershed)	Summary (Points)	K-S test
1	**Flow Line Curvature (radians m^{-1}):** The mean local curvature of pixels from a flow path running through a target pixel.	Min: -3.8e-3 Max: 3.4e-3 Mean: -3.4e-6 SD: 1.7e-4	Min: -4.3e-4 Max: 5.6e-4 Mean: 7.9e-6 SD: 2.2e-4	D: 0.20 p: 0.40
2	**Topographic Wetness Index (SAGA):** A SAGA modified version of the Topographic Wetness Index (Beven and Kirkby, 1979) that also accounts for vertical distance to the channel network.	Min: 2.1 Max: 12.6 Mean: 5.8 SD: 1.8	Min: 3.5 Max: 10.4 Mean: 5.9 SD: 2.2	D: 0.23 p: 0.26
3	**Slope (radians):** The angle of maximum rise over run at each pixel.	Min: 2.7e-4 Max: 0.43 Mean: 0.11 SD: 0.07	Min: 0.04 Max: 0.35 Mean: 0.17 SD: 0.08	D: 0.47 p: <0.01
4	**Channel Network Base Level (masl):** The interpolated elevation of a stream channel network.	Min: 77.1 Max: 101.4 Mean: 91.0 SD: 5.3	Min: 78.4 Max: 92.6 Mean: 85.4 SD: 3.9	D: 0.48 p: <0.01
5	**Vertical Distance to Channel Network (m):** The difference between surface elevation and Channel Network Base Level.	Min: 0 Max: 15.4 Mean: 3.8 SD: 3.4	Min: 0 Max: 9.5 Mean: 3.0 SD: 3.0	D: 0.15 p: 0.74
6	**Downslope Curvature (radians m^{-1}):** The mean local curvature of pixels along the downslope flow path running from a given pixel.	Min: -0.59 Max: 0.22 Mean: -0.01 SD: 0.05	Min: -0.19 Max: 0.07 Mean: -0.03 SD: 0.06	D: 0.25 p: 0.16
7	**Upslope Accumulation Area (m^2):** The area of pixels that are routed through a given pixel by a flow direction calculation (m^2)	Min: 11 Max: 47300 Mean: 945 SD: 2740	Min: 54 Max: 13100 Mean: 1850 SD: 3518	D: 0.24 p: 0.19
8	**Aspect (radians away from 0 (North)):** The direction of a slope. In this case, aspect has been normalized such that maximum values are south-facing and minimum values are north facing	Min: 0 Max: 3.1 Mean: 2.1 SD: 1.4	Min: 1.2 Max: 3.1 Mean: 2.1 SD: 1.2	D: 0.20 p: 0.43
9	**Catchment Slope (radians):** The mean slope angle of pixels within an Upslope Accumulation Area.	Min: 3.8e-4 Max: 0.30 Mean: 0.09 SD: 0.04	Min: 0.09 Max: 0.20 Mean: 0.14 SD: 0.03	D: 0.58 p: <0.01
10	**Multiresolution Index of Valley Bottom Flatness:** A quantitative measure of valley bottom topographic characteristics based of slope angles of a pixel derived at multiple resolutions (Gallant and Dowling, 2003).	Min: 0 Max: 4.8 Mean: 0.55 SD: 0.60	Min: 0 Max: 1.4 Mean: 0.29 SD: 0.46	D: 0.43 p: <0.01
11	**Multiresolution Index of Ridge Top Flatness:** A quantitative measure of upland plateau topographic characteristics based of slope angles of a pixel derived at multiple resolutions (Gallant and Dowling, 2003).	Min: 0 Max: 4.0 Mean: 0.38 SD: 0.59	Min: 0 Max: 0.95 Mean: 0.09 SD: 0.21	D: 0.48 p: <0.01

soil GHG flux) as a function of its predictors (i.e., terrain attributes). Therefore, quantile regression forests provide the means to judge the reliability of predictions, since prediction intervals can be extracted from the full conditional distribution of both predicted fluxes at each season for each pixel across the watershed. After variable selection, quantile regression forest model parameters *mtry* (the number of predictor variables randomly selected at each node in a tree) and *ntree* (the number of "trees" grown in the forest) were tested using leave-one-out cross validation to minimize model error while maximizing explained variance. The *mtry* parameter was tested from 2 to n – 1 (n = number of predictors), and the *ntree* parameter was tested from 50 to 1000 at increments of 10. The result of the quantile regression forest was a set of conditional prediction distributions (*ntree* ranged 90 to 230 for CO_2 fluxes and 60 to 230 for CH_4 fluxes) of mean mid-day soil CO_2 and CH_4 fluxes at each pixel (total of 30134) within the study watershed during each season. As these prediction distributions often were not normally distributed, medians of the conditional prediction distributions at each pixel were used as final predictions. The interquartile ranges of the conditional distributions were used as a spatially explicit measure of prediction uncertainty. This approach allowed us to predict spatially continuous distributions of seasonal mean mid-day soil-atmosphere CO_2 and CH_4 fluxes and the interquartile range of these predictions across the 12 ha watershed for each season.

Variable selection, parameter testing, and quantile regression forest predictions were performed in packages "VSURF" (Genuer et al. 2016), "e1071" (Meyer et al. 2015), "randomForest" (Liaw and Wiener 2002), and "quantregForest" (Meinshausen 2016) in the R software (R Core Team 2015). Model accuracy was evaluated for each soil GHG flux and each season based on root mean square error (RMSE) and the coefficient of determination (r^2). Per hectare fluxes were estimated as the sum of the predicted fluxes at each 2-meter pixel multiplied by the true surface area (adjusted by slope) of each pixel and normalized to watershed area.

In this study, model performance and soil GHG predictions were evaluated in two ways. First was "model accuracy" referred to the coefficient of determination (r^2) and root mean square error (RMSE) of our quantile regression forests model fit to our 20 observations of each GHG flux in each season. Second was "prediction uncertainty", which referred to the spread of the conditional prediction distribution (where n = the *ntree* parameter) generated by the quantile regression forests model at each pixel. Thus, "model accuracy" was used as an indicator of overall model fit, while "prediction uncertainty" was used as an indicator of the consistency of predictions made by individual trees grown within the quantile regression forests model. Prediction uncertainty was expressed both as a percentage (i.e., interquartile range of the conditional prediction distribution divided by the median) and as a unit (i.e., μmol m^{-2} s^{-1} or nmol m^{-2} s^{-1}) value equal to the interquartile range of the conditional prediction distribution.

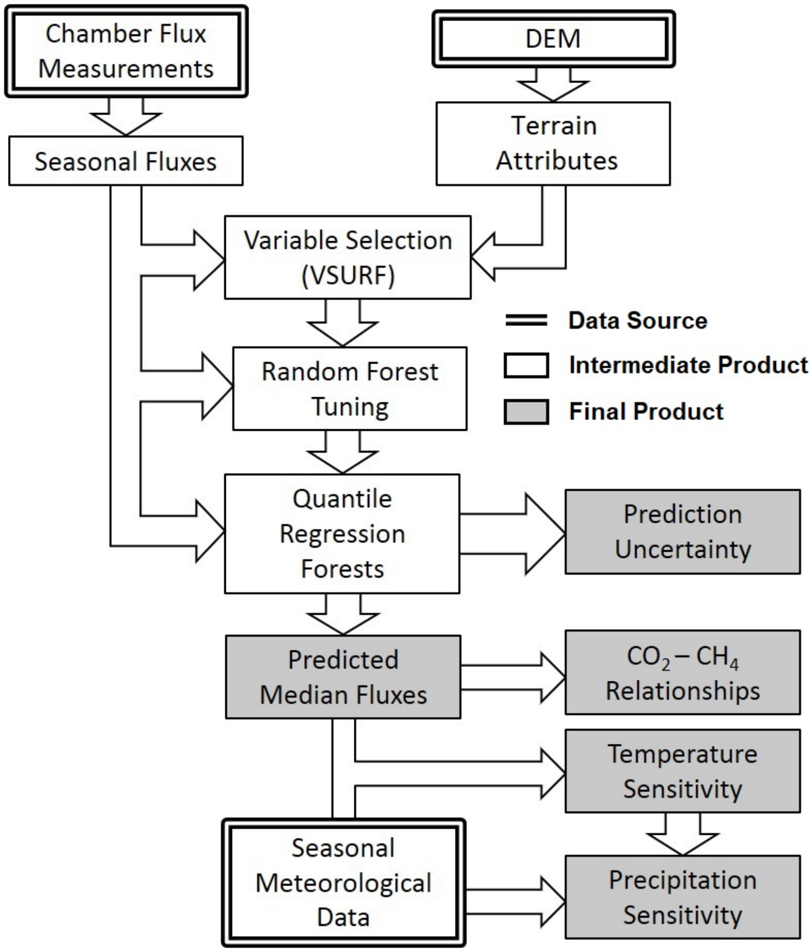

Figure 2. Flow diagram of modeling approach used in this study. Double outlines indicate primary data sources, while shaded boxes indicate final products presented in this paper.

2.5 Seasonal relationships of fluxes, temperature, and precipitation

To examine the watershed scale spatial variability of flux responses to seasonal climate patterns, we fit linear models to mean annual temperature and fluxes at each pixel. Seasonal meteorological data were taken from a nearby (~1 km) weather station in the Delaware Environmental Observation System (DEOS 2017). Temperature relationships to CO_2 and CH_4 fluxes were assessed by fitting pixel-wise linear models of mean seasonal air temperature to mean seasonal GHG fluxes and extracting the slope for each pixel, yielding a seasonal temperature relationship in units of μmol CO_2 m^{-2} s^{-1} or nmol CH_4 m^{-2} s^{-1} per degree Celsius. We also examined the potential influence of seasonal precipitation patterns on fluxes. In pixels where temperature-flux relationships were significant, the residuals of these relationships were related to mean weekly precipitation for each season. In pixels where temperature-flux relationships were not significant, predicted flux values were related to mean weekly precipitation in each season instead. Pixel-wise linear models were also used to examine relationships between CO_2 and CH_4 fluxes across seasons.

3. Results

3.1 Selected variables for each season and gas flux

A total of 10 prediction grids were made (one for each season and each gas), and the selected predictor variables were different between seasons and between CO_2 and CH_4 fluxes. Table 2 lists which variables were selected for each model. A topographic wetness index was selected as a predictor of CH_4 fluxes across all seasons, and as a predictor for CO_2 from early summer to fall. Flow line curvature was selected as a predictor for CO_2 fluxes in all seasons, but never for CH_4 fluxes. Slope angle, upslope accumulation area, and the Multiresolution index of

Valley Bottom Flatness (MRVBF) were also commonly selected as predictors of CH_4 fluxes, while upslope accumulation area and the interpolated channel network base elevation were selected in three seasons for CO_2 fluxes. Other variables, such as aspect, were selected only once for a specific season and flux (Table 2).

3.2 Predicted fluxes and model accuracy

Model predictions of mean mid-day fluxes were close to our observed mean fluxes across sampling locations in each season (Fig 3). A detailed description of observed fluxes can be found in Warner et al. (2018). Model accuracy was lowest in spring for both CO_2 and CH_4 with r^2 of 0.1 and 0.35, and RMSE of 0.39 μmol CO_2 m^{-2} s^{-1} and 0.25 nmol CH_4 m^{-2} s^{-1}, respectively. Model accuracy was highest in early summer for CO_2 ($r^2 = 0.61$, RMSE = 0.90 μmol m^{-2} s^{-1}) and in late summer for CH_4 ($r^2 = 0.64$, RMSE = 0.47 nmol m^{-2} s^{-1}). A list of model r^2 and RMSE is provided in Table 2.

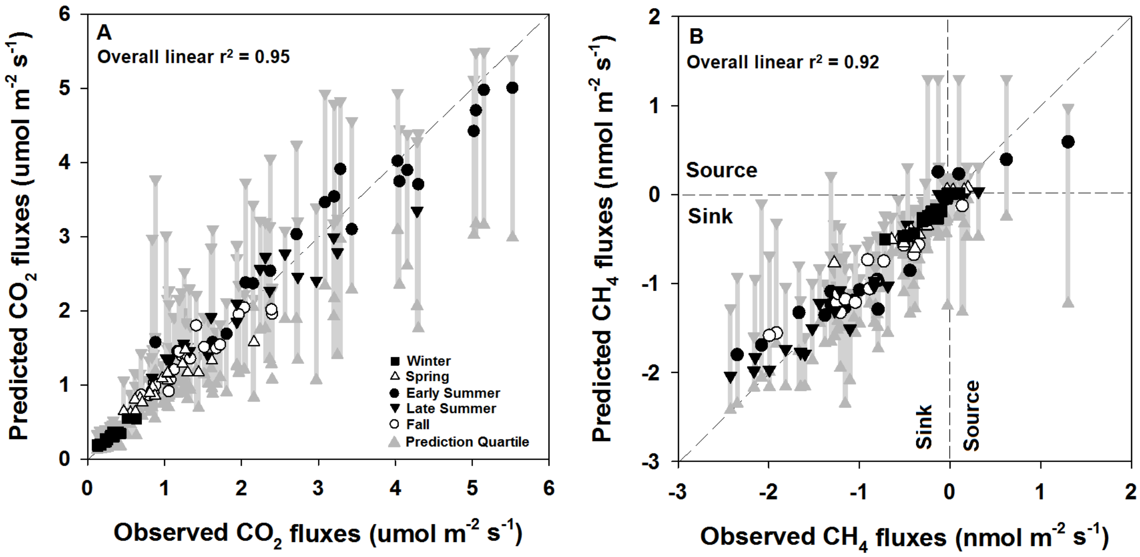

284

285 Figure 3. Comparisons of observed CO_2 and CH_4 fluxes and predicted fluxes from the medians
286 of conditional prediction distributions generated by quantile regression forests. In panels A and
287 B, seasons are denoted by shapes, and error bars indicate the upper and lower quartiles of the
288 conditional prediction distributions.
289

290 Table 2. R-squared and Root Mean Square Error values for assessing model accuracy of quantile
291 regression forests models. Selected variables for each model correspond to the ID Number
292 column of Table 1.

	CO_2 fluxes			CH_4 fluxes		
Season	**R^2**	**RMSE (µmol m^{-2} s^{-1})**	**Variables Selected**	**R^2**	**RMSE (nmol m^{-2} s^{-1})**	**Variables Selected**
Winter	0.42	0.09	1, 4, 6, 8, 9	0.57	0.13	2, 7, 10
Spring	0.10	0.39	1, 5, 11	0.35	0.25	2, 3, 7, 10
Early Summer	0.61	0.90	1, 2, 4, 7	0.50	0.60	3, 7
Late Summer	0.40	0.70	1, 2, 3, 4	0.64	0.47	2, 3, 10
Fall	0.40	0.39	1, 2, 7	0.39	0.46	2, 10

293

Like the observed GHG fluxes, predicted seasonal mean fluxes varied across the landscape and across seasons (Fig 4). Predicted CO_2 efflux was generally low in winter (range 0.15 to 0.55 μmol m^{-2} s^{-1}), with the highest fluxes in the steep south-facing slopes near the watershed outlet, and lowest in low slope pixels near the stream network and in the upper reaches of the watershed. Winter predictions of net CH_4 uptake were highest along convergent hillslopes (maximum -0.52 nmol m^{-2} s^{-1}), with neutral to slightly positive net CH_4 fluxes predicted in low lying areas (Fig 4). In spring, predicted CO_2 efflux was highest in steeply sloping and low slope pixels that that were situated high above the stream channel (range 0.60 to 1.6 μmol m^{-2} s^{-1}). Predicted CH_4 uptake was highest on the steepest areas of the catchment in spring (maximum -0.81 nmol m^{-2} s^{-1}), with neutral to slightly positive soil CH_4 fluxes predicted in flat, near stream areas of the watershed (Fig 4). Early summer predicted mean CO_2 efflux was the highest of any season (maximum of 5.2 μmol m^{-2} s^{-1}) in steep sloping pixels near the watershed outlet, especially in pixels with concave flow line curvature. However, low CO_2 efflux (minimum of 1.4 μmol m^{-2} s^{-1}) was predicted in low slope pixels near the stream network. Early summer also had the highest predicted soil CH_4 emissions (maximum of 0.6 nmol m^{-2} s^{-1}), which corresponded to areas of very low predicted CO_2 efflux. Low soil CH_4 uptake (~ -0.2 nmol m^{-2} s^{-1}) was predicted for most of the watershed except in pixels with high slopes and low upslope area, where predicted soil CH_4 uptake was relatively high (maximum of -1.9 nmol m^{-2} s^{-1}) (Fig 4). In late summer, predicted CO_2 efflux was again highest in high slope pixels, but without the same small areas of relatively high efflux observed in early summer. CO_2 efflux was relatively small across the rest of the watershed (range 1.1 to 3.4 μmol m^{-2} s^{-1}). Predicted net CH_4 uptake was highest during this season, with the highly negative values concentrated along convergent hillslopes (maximum of -2.1 nmol m^{-2} s^{-1}), slightly negative values in low slope areas above and below the hillslopes, and slightly positive soil CH_4 fluxes in flat areas surrounding the stream network. Predicted CO_2 efflux and CH_4 uptake was slightly lower across the watershed in fall than in late summer, but the spatial patterns of the highest predicted fluxes were similar between the two seasons. Most notably, positive CH_4 fluxes were not predicted in any pixels during these seasons (Fig 4).

3.3 Prediction uncertainty

Percent prediction uncertainty (the interquartile range of the prediction distribution at each pixel as a percentage of the median of the prediction distribution) of predicted CO_2 efflux was relatively low compared to predicted CH_4 fluxes (Fig 5), generally staying below 100% across all seasons. For CO_2 efflux, spatial distributions of areas with relatively high percent prediction uncertainty varied between seasons. Areas of high percent prediction uncertainty were focused in low slope pixels high above the stream network (winter and spring), steep near stream areas (early summer), flat pixels near the watershed outlet (late summer), but were scattered across the watershed in fall (Fig 5). Predicted CH_4 fluxes had very large ranges in percent uncertainty, but the spatial patterns of this uncertainty were more consistent across seasons than for CO_2 predictions. Percent uncertainty for each prediction was relatively low (< 100%) in high slope pixels during all seasons, but extremely high percent uncertainty (> 1000%) was observed for CH_4 fluxes in some areas with near-zero predicted net fluxes (Fig 5, 6). In general, percent prediction uncertainty was highest in pixels where predicted fluxes were nearest to zero, although low predicted fluxes were often associated with similarly low prediction uncertainty in units of flux (Fig 6). In exception, soil CH_4 flux predictions were highly uncertain in low slope pixels in upland areas of the watershed during early summer, resulting in high percent uncertainty in many of pixels predicted to be moderate sinks or sources of CH_4 (Fig 5, 6).

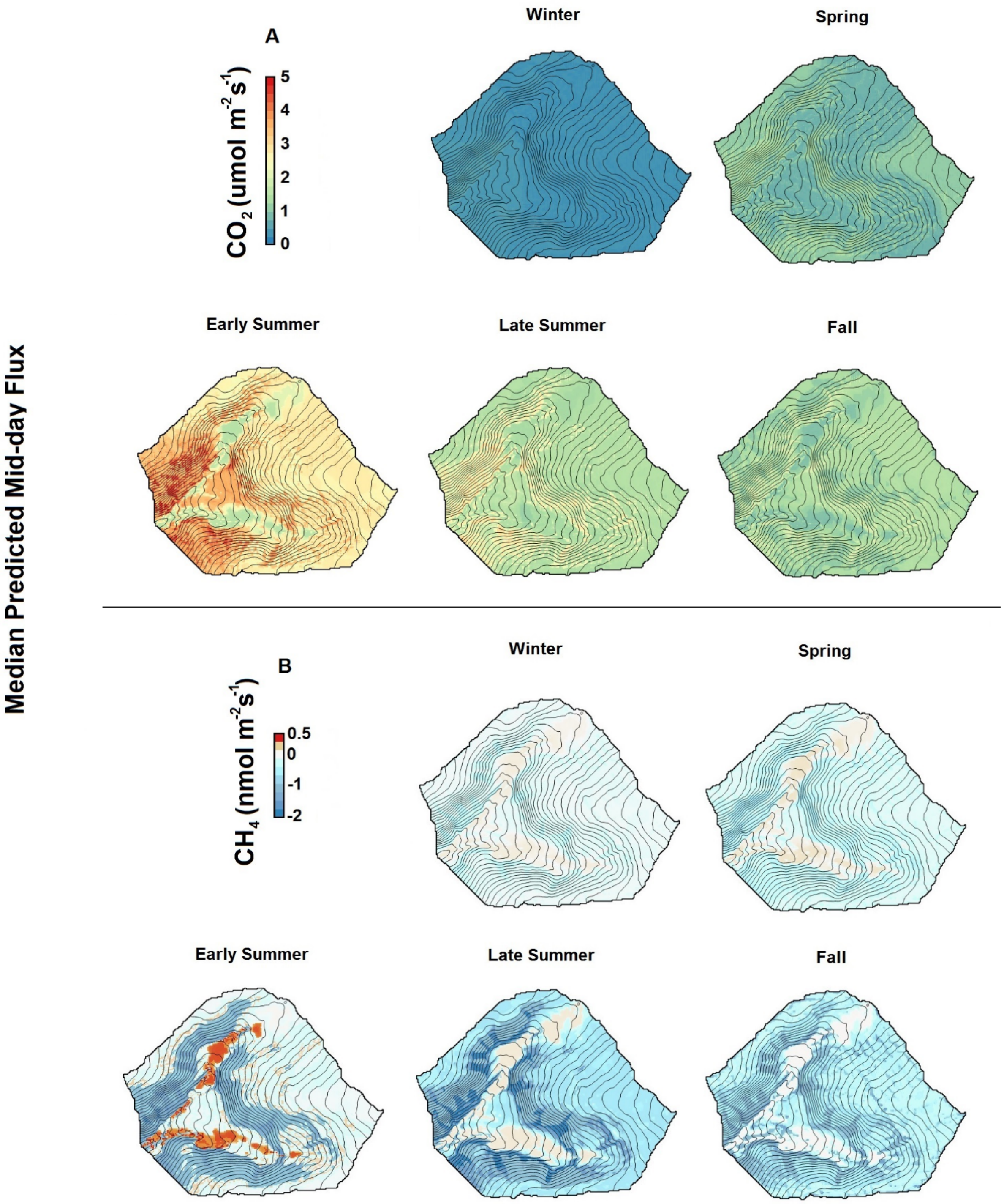

Figure 4. Predicted seasonal mean mid-day CO_2 (top) and CH_4 (bottom) fluxes at each pixel in our study watershed during each season. Predicted values represent the median of the conditional prediction distribution of seasonal mean fluxes generated for each pixel.

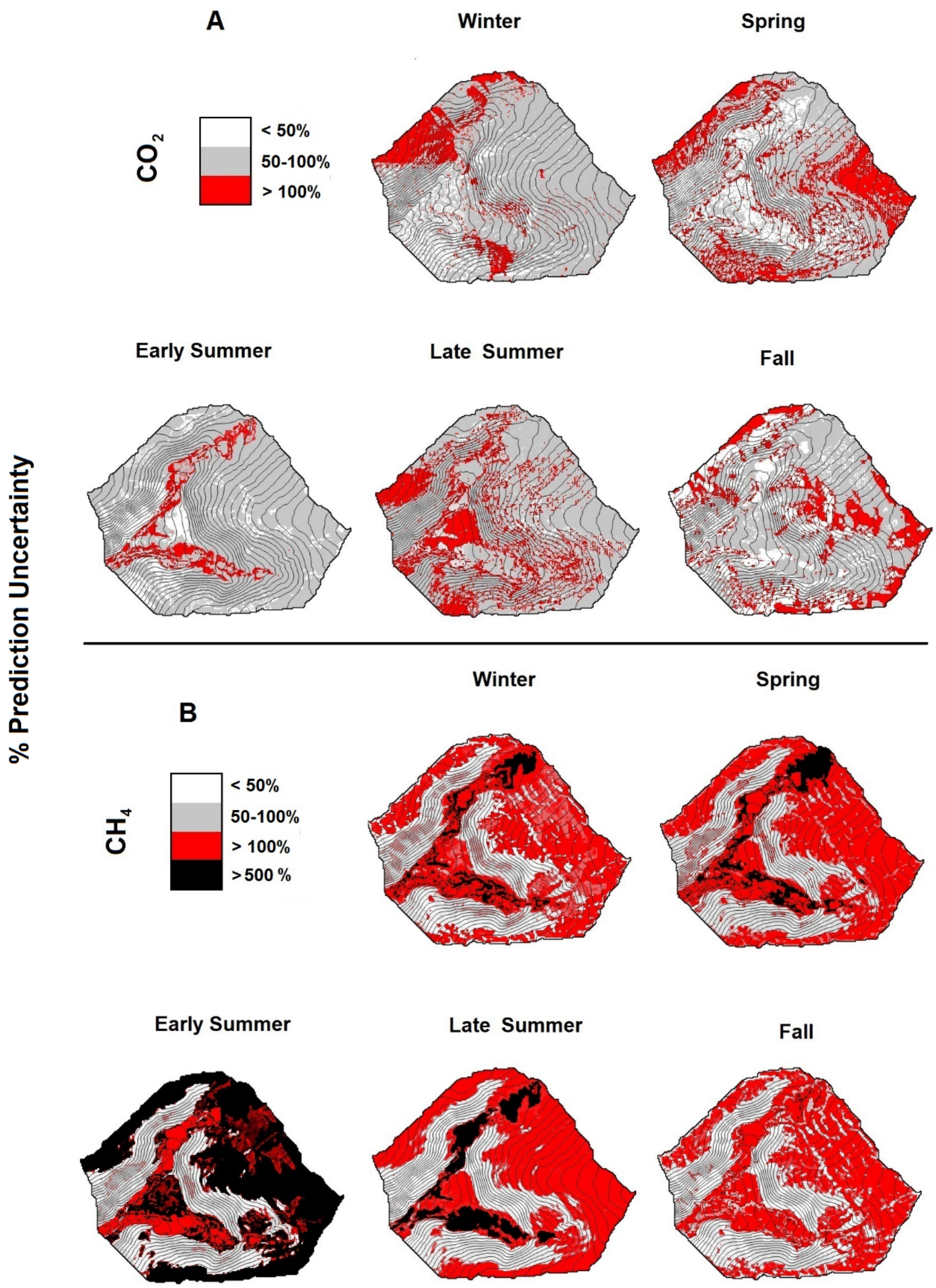

Figure 5. Percent prediction uncertainty for CO_2 (top) and CH_4 (bottom) fluxes at each pixel in our study watershed during each season. Percent uncertainty was calculated as the interquartile range divided by the median of the conditional prediction distribution generated for each pixel.

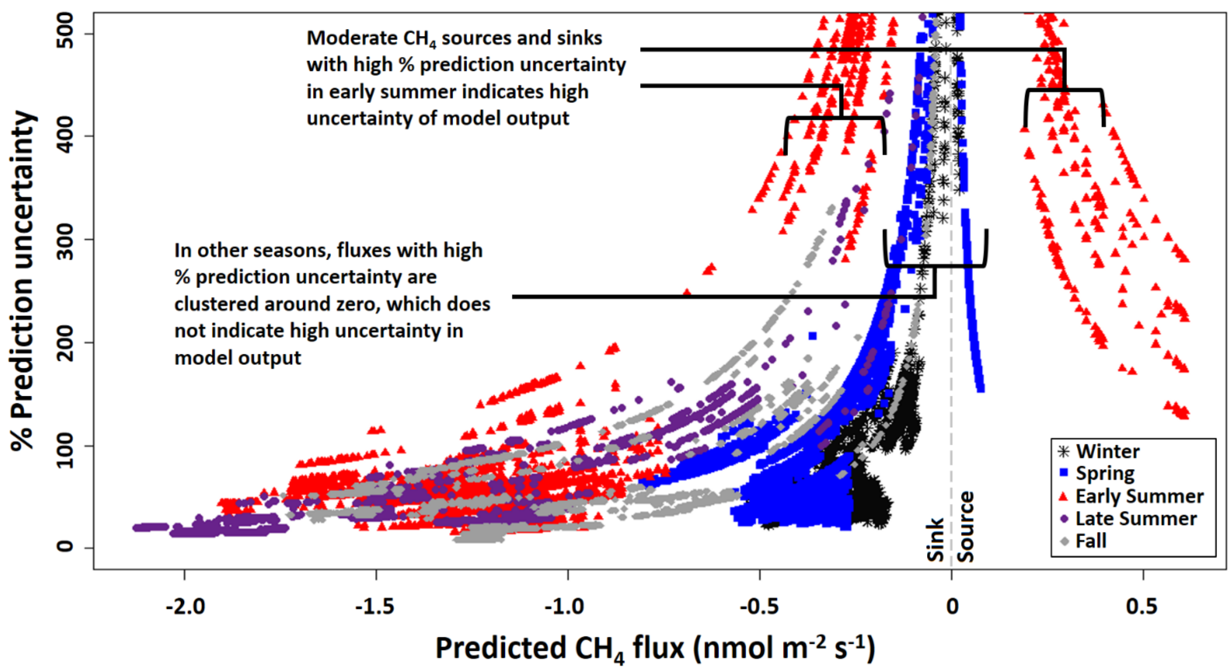

Figure 6. The relationship between % prediction uncertainty and predicted CH_4 fluxes. High % prediction uncertainty is caused by some of the uncertain model predictions of CH_4 fluxes in early summer, while in other seasons it is due to near-zero predicted CH_4 fluxes.

3.4 Per hectare fluxes and whole watershed means

We predicted the mean mid-day flux per hectare of both gases as the sum of predicted fluxes at each pixel divided by watershed area. Per hectare CO_2 emissions were greatest in early summer, with predicted mean mid-day efflux (sum of lower and upper quartiles of prediction distribution) of 108 (73.1 to 150) mol CO_2 hr^{-1} ha^{-1}. Early summer predicted CH_4 fluxes had the greatest uncertainties, leading to predicted mean mid-day net flux of -17.1 (-53.8 to 21.8) mmol CH_4 hr^{-1}. Predicted per hectare net CH_4 flux was greatest in late summer and fall, with fluxes of -29.5 (-51.8 to -6.3) and -22 (-41.4 to -6.4) mmol CH_4 hr^{-1}, respectively. Fluxes were lowest during winter months, with estimated per hectare mid-day fluxes of 10.0 (5.6 to 14.8) mol CO_2 hr^{-1} and -5.9 (-11.3 to -0.6) mmol CH_4 hr^{-1} . When comparing CO_2 equivalents using a 100-year global warming potential of 25 for CH_4, we estimated that soil CH_4 fluxes could offset the global warming potential of CO_2 efflux by 1.5% (2.8 - 0.5%) in winter, 0.4% (1.3 - +0.5%) in early summer, and 1.2% (2.1 - 0.3%) in late summer.

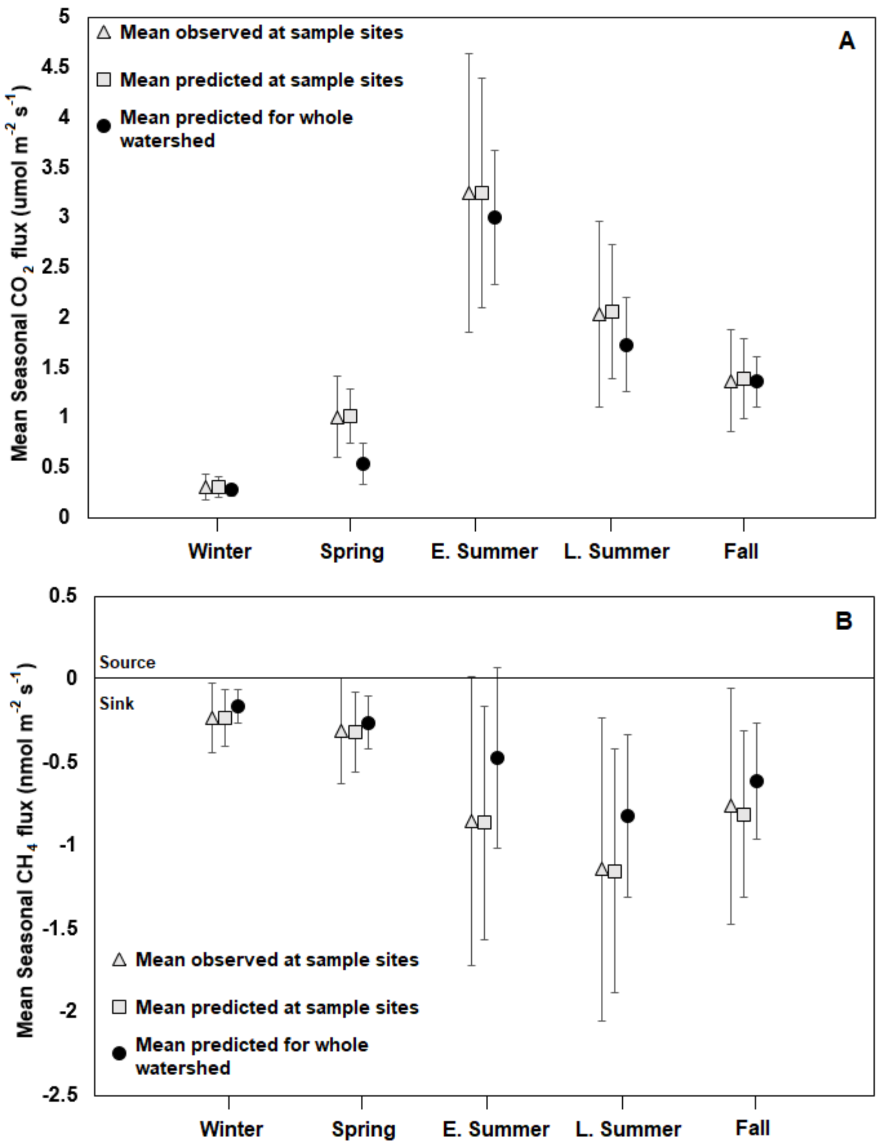

Figure 7. Comparisons of seasonal means (± 1 S.D.) of observed fluxes at sampling locations (grey triangles, n = 20), predicted fluxes at sampling locations (grey squares, n = 20), and predicted fluxes across the entire study watershed (black circles, n = 30134).

We compared the means of observed fluxes across the 20 sampling sites to means of predicted fluxes at 20 sampling sites and across the whole study watershed (Fig 7). Observations and predictions at the 20 sampling sites were generally quite close. Mean predicted CO_2 efflux across the whole watershed was lower than the means of predictions and observations at the 20 sampling locations in spring (Fig 7a). From early summer to fall, mean predicted CH_4 uptake across the whole watershed was lower than the means of predictions and observations at the 20 sampling locations (Fig 7b).

3.5 Seasonal relationships between fluxes, temperature, and precipitation

Linear models relating seasonal mean air temperature (explanatory variable) with predicted seasonal mean CO_2 efflux (response variable) were significant ($p < 0.05$) at every pixel in the watershed. The slopes of these relationships ranged from 0.2 to 0.6 μmol CO_2 m^{-2} s^{-1} $^{o}C^{-1}$ with lower values found in flat near stream areas and higher values found along steep slopes, with the highest values corresponding to areas of extremely high predicted efflux in early summer (Fig 4, 8a). Linear models relating seasonal mean soil CH_4 fluxes and temperature were significant ($p < 0.05$) within pixels on steep sloping areas and in a few scattered pixels in other parts of the watershed, but were not significant for most pixels with low slope values. Where significant, slopes of temperature relationships ranged from -0.23 to -0.02 (nmol CH_4 m^{-2} s^{-1} $^{o}C^{-1}$), with the greatest relationship for soil CH_4 uptake across sloped convergent zones and along the base of steeply sloping areas (Fig 8b).

There were no significant relationships between precipitation and the residuals of the CO_2-temperature relationships in any pixel, nor were there any such relationships with CH_4-temperature residuals in the pixels where these relationships were significant. However, mean weekly precipitation was significantly positively correlated to soil CH_4 fluxes (higher net

CH_4 emissions in wet seasons) in low slope pixels near the stream network (~ 0.07 nmol CH_4 m^{-2} s^{-1} mm^{-1}), and negatively correlated in similarly low slope pixels at the perimeter of these areas (~ -0.07 nmol CH_4 m^{-2} s^{-1} mm^{-1}), (Fig 8c).

Seasonal CO_2 and CH_4 fluxes were significantly correlated to each other for a small portion of the watershed that primarily included the same pixels where significant CH_4 – temperature relationships were observed (Fig 8d). This correlation was generally negative where it was significant, indicating a seasonal increase in soil CH_4 uptake with increasing CO_2 efflux.

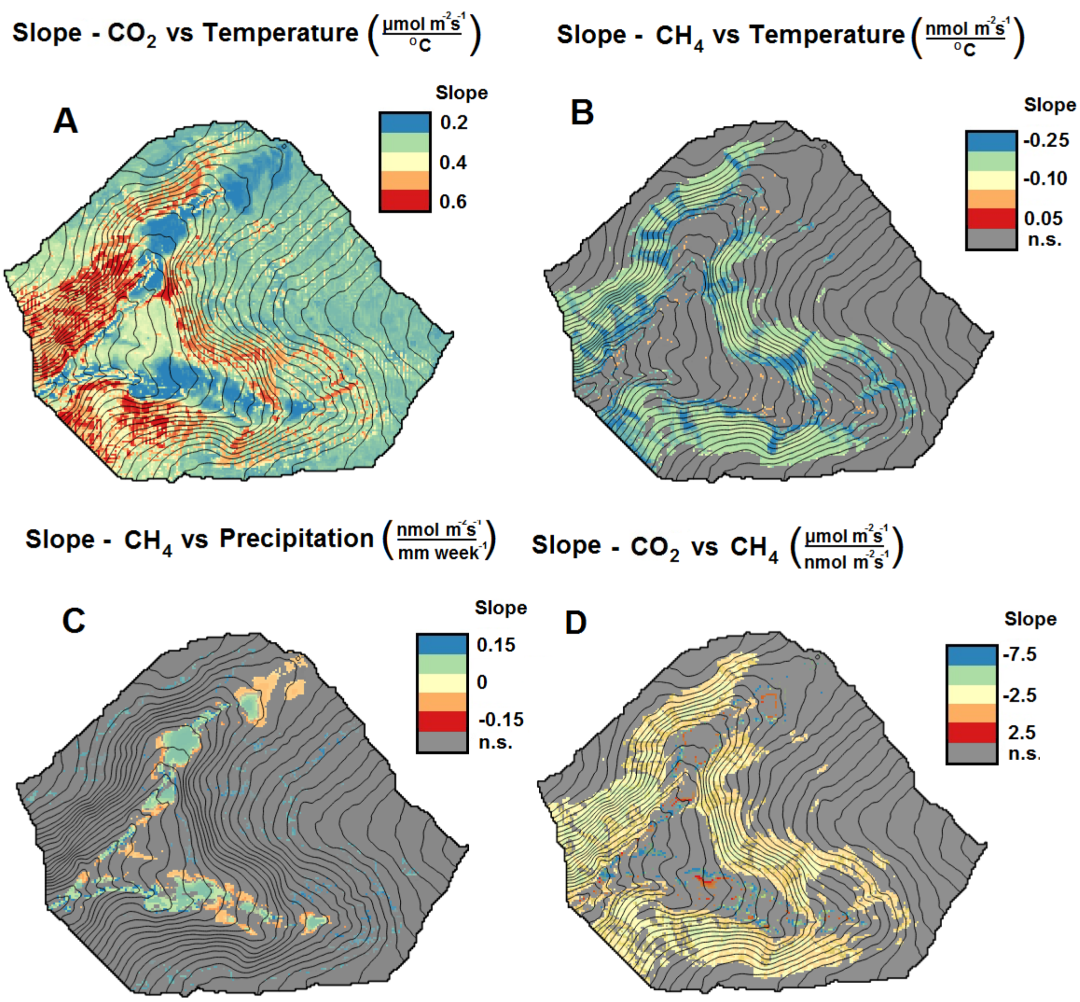

Figure 8. Pixel-wise slopes derived from linear models of seasonal (B) CO_2 and seasonal mean temperature, (C) CH_4 fluxes and seasonal mean temperature, (C) seasonal CH_4 fluxes and seasonal mean weekly precipitation, (D) seasonal mean CO_2 fluxes and CH_4 fluxes. Gray areas indicate pixels with non-significant (n = 5, p > 0.1) relationships.

4. Discussion

4.1 Continuously distributed flux predictions

This study demonstrates that a digital soil mapping framework can be used to predict soil-atmosphere CO_2 and CH_4 fluxes across a forested watershed. Predicted mean fluxes from quantile regression forests closely represented our observations in all seasons (Fig 3), suggesting that soil surface GHG flux measurements and DEM-derived terrain attributes can be effectively used in tandem to estimate soil-atmosphere fluxes across topographically heterogeneous ecosystems. Unlike approaches that rely on classification and aggregation of fluxes from major landforms (Gomez et al., 2016; Webster et al., 2008a), this approach allowed us to estimate the continuous spatial distributions of these fluxes at high spatial resolution (2 m pixel size). Though both approaches can discern differences in fluxes between major landscape features (i.e., hillslopes, upland and valley bottom flats), our approach also provided a detailed, continuous estimate of flux variability *within* major landscape features that cannot be achieved by only using landform classification. For example, our approach suggested the elevated CO_2 efflux in areas of concave flow line curvature along transitional hillslopes in early summer, and elevated CH_4 uptake along convergence zones along transitional hillslopes in late summer and fall (Fig 4). The elevated patches of CO_2 efflux may be a result of organic carbon accumulation in areas of concave hillslope curvature (Fissore et al., 2017) coupled with hot, moist conditions in the early summer season, which would be conducive for high rates of heterotrophic respiration. The predicted elevated rates of CH_4 uptake in convergence zones along hillslopes is noteworthy, as these were areas with higher topographic wetness indices (representing where water would tend to accumulate) than other parts of the hillslopes. Soil moisture is generally assumed to inhibit methanotrophic activity because it limits O_2 and CH_4 diffusion into the soil (Del Grosso et al.

2000), but it is possible that these convergence areas remain moist enough to protect soil microbial communities from drought stress during dry seasons like late summer and fall, allowing elevated CH_4 uptake at these times.

The ranges of our flux predictions were comparable to fluxes reported in other temperate forests. Our CO_2 efflux predictions fell within the ranges reported in another temperate forest, which ranged from a median of 0.7 μmol CO_2 m^{-2} s^{-1} in winter/spring to 4.1 μmol CO_2 m^{-2} s^{-1} in summer, with high emissions in along hillslopes and low emissions in flatter, low lying areas (Creed et al., 2013; Webster et al., 2008b). Our predictions of net CH_4 fluxes were also comparable to observations in a similar temperate forest, that found mean late summer net CH_4 fluxes of -2.0 nmol CH_4 m^{-2} s^{-1} in slopes and flat upland areas, but high emissions of CH_4 (some instantaneous measurements as high as 100 nmol CH_4 m^{-2} s^{-1}) only during early summer in flay, low lying areas of the watershed (Wang et al., 2013). While our predicted mean CH_4 efflux only reached a maximum of 0.6 nmol CH_4 m^{-2} s^{-1}, we too observed brief "hot moments" of emissions in early summer (as high as 19 nmol CH_4 m^{-2} s^{-1}) in low lying flat areas near the stream network, which had near-zero net fluxes during the rest of the year (Warner et al., 2018).

4.2 Mean flux predictions and uncertainty

In most seasons, mean predicted CO_2 fluxes for the whole study watershed were similar to mean observed and predicted fluxes for the 20 sampling locations (Fig 7a). This suggests that the sampling locations in this study were able to represent the general distribution of CO_2 fluxes across the catchment for most seasons except spring, when the 20 sampling points may have overrepresented areas with high CO_2 emissions. Similarly, the 20 sampling points may have overrepresented areas of high CH_4 uptake during the summer and fall (Fig 7b). These results demonstrate how mean fluxes at the watershed or landscape scale may be influenced not only by spatial variability across the land surface, but by seasonal variability in spatial patterns of fluxes. The representativeness of a set of chamber measurement locations may inconsistent in time, as the spatial patterns of fluxes vary with seasons. Our findings suggest that spatially continuous approaches for scaling flux observations may help reduce such temporally transient biases when making large scale estimates of flux means and totals based on static chamber measurements across complex landscapes.

The spatial distributions of prediction uncertainty may also vary from season to season. This was very clear for predictions of early summer CH_4 fluxes. Model estimates of early summer CH_4 flux per hectare ranged from a moderate net source to a moderate net sink. We attribute this broad range to the large prediction uncertainties of CH_4 fluxes in some areas of the watershed during this season (Fig 5). We found two primary causes of high percent prediction uncertainty in our models. In some cases (such as in low-lying areas during late summer), the high percent CH_4 prediction uncertainty was a product of a prediction distribution with a median near zero and an interquartile range that, while small in units of flux, was much larger than the median prediction (for example, a median and interquartile range of 0.001 and 0.1 nmol m^{-2} s^{-1} would have a percent prediction uncertainty of 10000%; Fig 6). In early summer however, high percent prediction uncertainty was a product of highly variable conditional prediction distributions in some areas of the watershed (Fig 5, 6, early summer predictions), which led to a highly uncertain estimate of large scale soil CH_4 flux in early summer. It should be noted, however, that large scale measurement techniques like eddy covariance can face the same challenges when hotspots form in hot, wet conditions (Hörtnagl et al., 2018; Wang et al., 2013).

As ecosystem models continue to provide increasingly detailed insights into biogeochemical processes, communicating their uncertainty, and the underlying implications of this uncertainty, becomes increasingly important. In the former case described above, percent prediction uncertainty may be high, but the degree of this uncertainty in units of flux may be too small to be ecologically relevant. In the latter case, the high level of prediction uncertainty in flat, high elevation areas has major implications for interpreting the net CH_4 source or sink status of the landscape. Beyond communicating the uncertainty of model estimates, understanding the causes for this uncertainty may highlight certain processes are challenging to model (i.e. greenhouse gas fluxes), and help guide future efforts in upscaling chamber measurements.

The high uncertainty of per hectare early summer CH_4 fluxes may stem from the large variability of CH_4 fluxes within landscape features that have similar topographic characteristics (e.g., flat or low slope) in hot, wet environmental conditions. We observed large CH_4 emissions in a few low elevation sampling locations while other pixels with similar terrain attributes had no net flux, or were weak net sinks of CH_4. Studies in other temperate forests have observed brief early summer “hot moments” of CH_4 emissions from small areas of low-lying soils that may entirely offset or exceed CH_4 uptake occurring across most of the watershed (Itoh et al., 2007; Wang et al., 2013). Furthermore, it is known that anaerobic biogeochemical processes, such as methane production, can vary significantly in space due to subtle variations in surface microtopography at scales below the 2 meter scale employed in this study (Frei et al., 2012), which may help explain why CH_4 flux observations from different small-footprint chambers may vary significantly even within areas with similar DEM-derived terrain attributes. Our variable selection process selected only terrain attributes of slope and upslope accumulation area as predictors of CH_4 fluxes in early summer (Table 2). Slope was similarly low in pixels in flat areas near the stream network and in high elevation areas, while upslope accumulation area was variable in the former and low in the latter. Thus, in some cases our quantile regression forests model made predictions based on attributes of topographically similar pixels with distinctly different CH_4 fluxes, which led to highly variable conditional prediction distributions. Low slope pixels occupy a large portion of this study watershed, the high prediction uncertainty of these pixels was compounded in our per hectare flux estimates. These findings highlight the difficulties that "hot spots" and "hot moments" of CH_4 fluxes introduce to large scale modeling efforts (Savage et al., 2014). This could potentially be addressed by more frequent measurements and the use of larger footprint chambers, or larger numbers of chambers, in areas prone to forming biogeochemical hot spots (wet, low lying soils). Striking a balance between the logistical constraints of chamber flux measurement campaigns and the selection of sampling sites, duplicate measurements within pixels, and chamber size is challenging, and the successes and setbacks of this and future research efforts will help optimize sampling strategies.

While high variability of fluxes from topographically similar pixels can cause large prediction uncertainty, the same problem may arise when similar fluxes are observed from topographically distinct pixels. This effect may be responsible for the much lower model accuracy for spring CO_2 efflux ($r^2 = 0.1$; Table 2) than for any other season or flux. In this season, our variable selection process selected flowline curvature, multiresolution index of ridge top flatness, and vertical distance to channel network as predictors of CO_2 efflux. Many pixels occupying sloping areas of the watershed have high, low, and intermediate values of these attributes, while flatter, high elevation pixels have low, high, and high values, respectively. Despite these major differences in selected terrain attributes, many of these pixels had similar

CO_2 fluxes, and consequently the model had challenges relating fluxes with surficial terrain attributes.

4.3 Relationships of seasonal CO_2 and CH_4 fluxes, temperature, and precipitation

Temporal relationships between seasonal meteorological patterns and fluxes were different for each gas. The highest temperature-CO_2 efflux relationship corresponded to soils along steep pixel with concave flow line curvature near the catchment outlet, and relatively lower temperature-CO_2 efflux relationships were found in low slope areas lying both near the stream network and high above it (Fig 8a). The higher temperature-CO_2 efflux relationship from the steep sloping areas indicates the potential importance of these topographic features to landscape scale CO_2 budgets in a warmer future climate. The residuals of the temperature-CO_2 efflux relationship were not correlated to mean weekly precipitation in any pixel, suggesting that the temperature is the dominant regulator of the seasonal variability of soil CO_2 efflux across this watershed. However, it should be noted that this study was not in an arid or semiarid ecosystem, and that precipitation variability is a well-known major driver of the seasonal variability of soil CO_2 efflux in many ecosystem types (Riveros-Iregui et al., 2012; Stielstra et al., 2015; Takahashi et al., 2011, Vargas et al., 2012).

Conversely, pixels with high slopes and low wetness indices (strong net CH_4 sinks) were the only portions of the watershed where significant linear relationships between seasonal temperature and CH_4 fluxes were observed (Fig 8b). Sloping areas, specifically convergent zones along and at the base of slopes, showed increasing negative CH_4 fluxes (i.e., CH_4 sinks) in warmer seasons. Pixels that were consistently net CH_4 sources, or pixels with near-zero net CH_4 fluxes in most seasons, were not significantly related to seasonal temperature (Fig 8b). However, we found significant relationships between mean seasonal CH_4 fluxes and weekly precipitation in low-lying flat areas near the stream network. Notably, the pixels that were closest to the stream or ephemeral channels showed a positive relationship between seasonal mean precipitation and CH_4 flux (i.e. more CH_4 emission in wetter seasons), but opposite relationships were observed in pixels in the adjacent perimeter areas (Fig 8c). Similar patterns have been observed during rainy periods in temperate forests (Itoh et al., 2007), which has been explained by a frequent lateral influx of oxygen-rich water to valley bottom perimeter soils that is rapidly depleted before it reaches more central soils. This results in sustained saturation and significantly increased CH_4 production in the central areas, but also suppressed CH_4 production in the adjacent perimeter soils (Itoh et al., 2007).

In addition to the relationships between GHG fluxes and seasonal meteorological patterns, we also examined the potential seasonal correlations among the GHG fluxes . There has recently been increasing interest in the relationships between soil CO_2 and CH_4 fluxes across landscapes, which may provide insights into the shared functional controls of heterogeneous soil types, vegetation, and microbial community structure on multiple soil greenhouse gas fluxes within an ecosystem (Maier et al., 2017). In general, soils with high CO_2 efflux tend to have high CH_4 uptake, while soils with low CO_2 efflux may have near-zero CH_4 fluxes or act as net sources of CH_4 (Maier et al., 2017; Warner et al., 2018). We found significant correlations between predicted seasonal CO_2 and CH_4 fluxes almost exclusively in steep sloping pixels (Fig 8d), the same areas where we found significant correlations between predicted CH_4 uptake and temperature. These sloped soils are generally well-aerated and well-drained, which consistently provides conditions conducive for aerobic heterotrophic activity and methane oxidation even in periods of frequent rain. Flatter and lower elevation areas of the watershed may be less well-drained, creating a soil environment that may be more conducive to CH_4 production, or may have a closer balance between methanogenic and methanotrophic processes. As rates of both methanogenesis and methanotrophy increase with temperature (Semenov et al., 2004; Yvon-Durocher et al., 2014), areas containing soils that support both microbial processes may have no relationship between temperature and the net CH_4 flux at the soil surface.

Thus, our findings suggest that warmer mean seasonal temperatures may influence steep slopes in forested ecosystems to act as relatively greater CO_2 sources, but also relatively greater net CH_4 sinks. However, changes in precipitation patterns may have a greater impact on CH_4 fluxes in flatter low lying areas than changes in seasonal temperatures, making the combined (and confounding) effects of temperature and precipitation variability on soil-atmosphere CH_4 exchange difficult to predict across topographically complex landscapes.

5. Conclusions

This study demonstrates the potential of digital soil mapping for making estimates of seasonal soil-atmosphere CO_2 and CH_4 fluxes across a topographically heterogeneous watershed based on manual soil flux measurements and publicly available topographic data. This approach worked well for predicting fluxes in most seasons, but predicted CH_4 fluxes had relatively higher uncertainty than predicted CO_2 efflux during early summer, when hotspots of CH_4 efflux developed in some areas in the watershed. We found areas with high slopes to have high relationship between temperature and CO_2 efflux and net CH_4 uptake, indicating the potential importance of soils on these landscape features to GHG budgets under future climate regimes. The well-drained soils of these slopes likely support aerobic soil processes across all seasons, resulting in a significant spatial correlation between CO_2 efflux and net CH_4 that was not observed in other areas of the watershed. Our approach also identified variability of fluxes within sloping areas of the landscape based on variations in terrain attributes, particularly in the summer and fall. The application of this digital soil mapping framework to existing chamber flux data or to future studies could provide insights about the spatial variability of soil GHG fluxes, the spatial variability of factors controlling them, and could aid the development of GHG budgets in complex terrain. We hope that this work encourages modeling efforts in other complex systems, which may need to incorporate publicly available data on vegetation, land use, and climate surfaces in addition to terrain attributes. Transparent communication of uncertainty, both in predictions and predictors, is important for allowing future studies to refine modeling efforts and estimates of greenhouse gas budgets in complex systems.

6. Acknowledgements

This study was funded by the US Department of Agriculture (USDA-AFRI Grant 2013-02758), and State of Delaware's Federal Research and Development Matching Grant Program. RV acknowledges partial support from the National Science Foundation (1724843, 1652594). We thank Samuel Villarreal and Shawn Del Percio for support during the field measurements.

7. References

Ambus, P., Christensen, S., 1995. Spatial and Seasonal Nitrous Oxide and Methane Fluxes in Danish Forest-, Grassland-, and Agroecosystems. J. Environ. Qual. https://doi.org/10.2134/jeq1995.00472425002400050031x

Anderson, R.H., Matthews, E.D., 1973. Soil Survey of Cecil County, Maryland. United States Department of Agriculture Soil Conservation Service, Washington, D.C.

Atkins, J.W., Epstein, H.E., Welsch, D.L., 2014. Vegetation heterogeneity and landscape position exert strong controls on soil CO2 efflux in a moist , Appalachian watershed. Biogeosciences 11, 17631–17673. https://doi.org/10.5194/bgd-11-17631-2014

Baldocchi, D., 2003. Assessing the eddy covariance technique for evaluating carbon dioxide exchange rates of ecosystems: past, present and future. Glob. Chang. Biol. 9, 479–492. https://doi.org/10.1046/j.1365-2486.2003.00629.x

Baldocchi, D.D., Finnigan, J., Wilson, K.B., U, K.T.P., Falge, E., 2000. On measuring net ecosystem carbon exchange over tall vegetation on complex terrain. Boundary-Layer Meteorol. 96, 257–291. https://doi.org/10.1023/A:1002497616547

Beven, K.J., Kirkby, M.J., 1979. A physically based, variable contributing area model of basin hydrology. Hydrol. Sci. Bull. https://doi.org/10.1080/02626667909491834

Breiman, L., 2001. Random forests. Mach. Learn. 45, 5–32. https://doi.org/10.1023/A:1010933404324

Conrad, O., Bechtel, B., Bock, M., Dietrich, H., Fischer, E., Gerlitz, L., Wehberg, J., Wichmann, V., Böhner, J., 2015. System for Automated Geoscientific Analyses (SAGA) v. 2.1.4. Geosci. Model Dev. https://doi.org/10.5194/gmd-8-1991-2015

Creed, I.F., Webster, K.L., Braun, G.L., Bourbonnière, R.A., Beall, F.D., 2013. Topographically regulated traps of dissolved organic carbon create hotspots of soil carbon dioxide efflux in forests. Biogeochemistry. https://doi.org/10.1007/s10533-012-9713-4

Crill, P.M., 1991. Seasonal patterns of methane uptake and carbon dioxide release by a temperate woodland soil. Global Biogeochem. Cycles 5, 319–334. https://doi.org/10.1029/91GB02466

Cueva, A., S. H. Bullock, E. Lopez-Reyes, and R. Vargas. 2017. Potential bias of daily soil CO_2 efflux estimates due to sampling time. Scientific Reports 7(11925). https://doi.org/10.1038/s41598-017-11849-y

Del Grosso, S.J., Parton, W., Mosier, A., Ojima, D.S., Potter, C.S., Brumme, R., Crill, P.M., Dobbie, K., Smith, K.A., 2000. General CH_4 oxidation model and comparisons of CH_4 oxidation in natural and managed systems. Global Biogeochem. Cycles 14:4, 999-1019. https://doi.org/ 10.1029/1999GB001226

Delaware Environmental Observing System (DEOS). 2017. Fair Hill NRMA Station. University of Delaware, Newark, DE, USA. www.deos.udel.edu Accessed: 03/15/17

Dlugokencky, E.J., Nisbet, E.G., Fisher, R., Lowry, D., 2011. Global atmospheric methane: budget, changes and dangers. Philos. Trans. A. Math. Phys. Eng. Sci. 369, 2058–2072. https://doi.org/10.1098/rsta.2010.0341

Fissore, C., Dalzell, B.J., Berhe, A.A., Voegtle, M., Evans, M., Wu, A., 2017. Influence of topography on soil organic carbon dynamics in a Southern California grassland. Catena 149, 140-149.

Frei, S., Knorr, K.H., Peiffer, S., Fleckenstein, J.H., 2012. Surface micro-topography causes hot spots of biogeochemical activity in wetland systems: A virtual modeling experiment. J. Geophys. Res. Biogeosciences. https://doi.org/10.1029/2012JG002012

Friedl, M.A., McIver, D.K., Hodges, J.C.F., Zhang, X.Y., Muchoney, D., Strahler, A.H., Woodcock, C.E., Gopal, S., Schneider, A., Cooper, A., Baccini, A., Gao, F., Schaaf, C., 2002. Global land cover mapping from MODIS: algorithms and early results. Remote Sensing of the Environ. 83, 287-302

Gallant, J.C., Dowling, T.I., 2003. A multiresolution index of valley bottom flatness for mapping depositional areas. Water Resour. Res. 39. https://doi.org/10.1029/2002WR001426

Genuer, R., Poggi, J., Tuleau-malot, C., 2012. Variable selection using Random Forests. Pattern Recognit. Lett. 31, 2225–2236.

Genuer, R., Poggi, J.M., Tuleau-Malot, C. 2016. VSURF: Variable selection using random forests. R package version 1.0.3.

Gomez, J., Vidon, P., Gross, J., Beier, C., Caputo, J., Mitchell, M., 2016. Estimating greenhouse gas emissions at the soil–atmosphere interface in forested watersheds of the US Northeast. Environ. Monit. Assess. 188, 295. https://doi.org/10.1007/s10661-016-5297-0

Gomez, J., Vidon, P., Gross, J., Beier, C., Mitchell, M., 2017. Spatial and Temporal Patterns of CO_2 , CH_4 , and N_2O Fluxes at the Soil-Atmosphere Interface in a Northern Temperate THE SCIENTIFIC PAGES Spatial and Temporal Patterns of CO O Fluxes at the Soil-Atmosphere Interface in a Northern Temperate Forested Watershed. Sci. Pages Res For. Watershed. Sci. Pages Res 1, 1–121.

Gomez, J., Vidon, P., Gross, J., Beier, C., Mitchell, M., 2017. Spatial and Temporal Patterns of CO_2 , CH_4 , and N_2O Fluxes at the Soil-Atmosphere Interface in a Northern Temperate Forested Watershed. Sci. Pages For. Res. 1, 1–12.

Gough, C.M., Vogel, C.S., Kazanski, C., Nagel, L., Flower, C.E., Curtis, P.S., 2007. Coarse woody debris and the carbon balance of a north temperate forest. For. Ecol. Manage. https://doi.org/10.1016/j.foreco.2007.03.039

Hengl, T., Heuvelink, G.B.M., Stein, A., 2004. A generic framework for spatial prediction of soil variables based on regression-kriging. Geoderma 120, 75–93. https://doi.org/10.1016/j.geoderma.2003.08.018

Hengl, T., Mendes de Jesus, J., Heuvelink, G.B.M., Ruiperez Gonzalez, M., Kilibarda, M., Blagotić, A., Shangguan, W., Wright, M.N., Geng, X., Bauer-Marschallinger, B., Guevara, M.A., Vargas, R., MacMillan, R.A., Batjes, N.H., Leenaars, J.G.B., Ribeiro, E., Wheeler, I., Mantel, S., Kempen, B., 2017. SoilGrids250m: Global gridded soil information based on machine learning, Plos One. https://doi.org/10.1371/journal.pone.0169748

Hörtnagl, L., Barthel, M., Buchmann, N., Eugster, W., Butterbach-Bahl, K., Díaz-Pinés, E., Zeeman, M., Klumpp, K., Kiese, R., Bahn, M., Hammerle, A., 2018. Greenhouse gas fluxes over managed grasslands in Central Europe. Global Change Biology 24(5), 1843-72.

Itoh, M., Ohte, N., Koba, K., Katsuyama, M., Hayamizu, K., Tani, M., 2007. Hydrologic effects on methane dynamics in riparian wetlands in a temperate forest catchment. J. Geophys. Res. Biogeosciences. https://doi.org/10.1029/2006JG000240

Jenson, S.K., Domingue, J.O., 1988. Extracting Topographic Structure from Digital Elevation Data for Geographic Information System Analysis. Photogramm. Eng. Remote Sensing 8825.

King, A.W., Andres, R.J., Davis, K.J., Hafer, M., Hayes, D.J., Huntzinger, D.N., De Jong, B., Kurz, W.A., McGuire, A.D., Vargas, R., Wei, Y., West, T.O., Woodall, C.W., 2015. North America's net terrestrial CO2 exchange with the atmosphere 1990-2009. Biogeosciences. https://doi.org/10.5194/bg-12-399-2015

Le Quéré, C., Andrew, R.M., Friedlingstein, P., Sitch, S., Pongratz, J., Manning, A.C., Korsbakken, J.I., Peters, G.P., Canadell, J.G., Jackson, R.B., Boden, T.A., Tans, P.P., Andrews, O.D., Arora, V.K., Bakker, D.C.E., Barbero, L., Becker, M., Betts, R.A., Bopp, L., Chevallier, F., Chini, L.P., Ciais, P., Cosca, C.E., Cross, J., Currie, K., Gasser, T., Harris, I., Hauck, J., Haverd, V., Houghton, R.A., Hunt, C.W., Hurtt, G., Ilyina, T., Jain, A.K., Kato, E., Kautz, M., Keeling, R.F., Klein Goldewijk, K., Körtzinger, A., Landschützer, P., Lefèvre, N., Lenton, A., Lienert, S., Lima, I., Lombardozzi, D., Metzl, N., Millero, F., Monteiro, P.M.S., Munro, D.R., Nabel, J.E.M.S., Nakaoka, S., Nojiri, Y., Padin, X.A., Peregon, A., Pfeil, B., Pierrot, D., Poulter, B., Rehder, G., Reimer, J., Rödenbeck, C., Schwinger, J., Séférian, R., Skjelvan, I., Stocker, B.D., Tian, H., Tilbrook, B., Tubiello, F.N., van der Laan-Luijkx, I.T., van der Werf, G.R., van Heuven, S., Viovy, N., Vuichard, N., Walker, A.P., Watson, A.J., Wiltshire, A.J., Zaehle, S., Zhu, D., 2018. Global Carbon Budget 2017. Earth Syst. Sci. Data 10, 405–448. https://doi.org/10.5194/essd-10-405-2018

Leon, E., Vargas, R., Bullock, S., Lopez, E., Panosso, A.R., La Scala, N., 2014. Hot spots, hot moments, and spatio-temporal controls on soil CO_2 efflux in a water-limited ecosystem. Soil Biol. Biochem. https://doi.org/10.1016/j.soilbio.2014.05.029

Liaw, A. and Weiner, M. 2002. Classification and regression by randomForest. R News 2(3); 18-22.

Maier, M., Paulus, S., Nicolai, C., Stutz, K., Nauer, P., 2017. Drivers of Plot-Scale Variability of CH_4 Consumption in a Well-Aerated Pine Forest Soil. Forests 8, 193. https://doi.org/10.3390/f8060193

McBratney, A.B., Mendonça Santos, M.L., Minasny, B., 2003. On digital soil mapping, Geoderma. https://doi.org/10.1016/S0016-7061(03)00223-4

Meinshausen, N., 2006. Quantile Regression Forests. J. Mach. Learn. Res. 7, 983–999. https://doi.org/10.1111/j.1541-0420.2010.01521.x

Meinshausen, N. 2016. quantregForest: Quantile regression forests. R package version 1.3.

Meyer, D., Dimitriadou, E., Hornik, K., Weingessel, A., Leisch, F. 2015. e1071: Misc functions for the department of statistics, probability theory group. R package version 1.6-7.

National Oceanic and Atmospheric Administration (NOAA). 2005. Coastal LiDAR Survey. Silver Spring, MD, USA.

Pan, Y., Birdsey, R.A., Fang, J., Houghton, R., Kauppi, P.E., Kurz, W.A., Phillips, O.L., Shvidenko, A., Lewis, S.L., Canadell, J.G., Ciais, P., Jackson, R.B., Pacala, S.W., McGuire, A.D., Piao, S., Rautiainen, A., Sitch, S., Hayes, D., 2011. A Large and Persistent Carbon Sink in the World's Forests. Science (80-.). https://doi.org/10.1126/science.1201609

Phillips, C.L., Bond-Lamberty, B., Desai, A.R., Lavoie, M., Risk, D., Tang, J., Todd-Brown, K., Vargas, R., 2017. The value of soil respiration measurements for interpreting and modeling terrestrial carbon cycling. Plant Soil 413, 1–25. https://doi.org/10.1007/s11104-016-3084-x

Phillips, S.C., Varner, R.K., Frolking, S., Munger, J.W., Bubier, J.L., Wofsy, S.C., Crill, P.M., 2010. Interannual, seasonal, and diel variation in soil respiration relative to ecosystem respiration at a wetland to upland slope at Harvard Forest. J. Geophys. Res. 115, 1–18. https://doi.org/10.1029/2008JG000858

Post, W.M., Emanuel, W.R., Zinke, P.J., Stangenberger, A.G., 1982. Soil carbon pools and world life zones. Nature. https://doi.org/10.1038/298156a0

R Core Team. 2015. R: A language and environment for statistical computing. R Foundation for Statistical Computing, Vienna, Austria. http://www.R-project.org/.

Raich, J.W., Potter, C.S., 1995. Global patterns of carbon dioxide emissions from soils. Global Biogeochem. Cycles 9, 23–36.

Raich, J.W., Tufekcioglu, A., 2000. Vegetation and soil respiration: Correlations and controls.

Biogeochemistry 48, 71–90.

Reyes, W.M., Epstein, H.E., Li, X., McGlynn, B.L., Riveros-Iregui, D.A., Emanuel, R.E., 2017. Complex terrain influences ecosystem carbon responses to temperature and precipitation. Global Biogeochem. Cycles 31, 1306–1317. https://doi.org/10.1002/2017GB005658

Riveros-Iregui, D.A., McGlynn, B.L., 2009. Landscape structure control on soil CO2 efflux variability in complex terrain: Scaling from point observations to watershed scale fluxes. J. Geophys. Res. Biogeosciences. https://doi.org/10.1029/2008JG000885

Riveros-Iregui, D.A., Mcglynn, B.L., Emanuel, R.E., Epstein, H.E., 2012. Complex terrain leads to bidirectional responses of soil respiration to inter-annual water availability. Glob. Chang. Biol. https://doi.org/10.1111/j.1365-2486.2011.02556.x

Saunois, M., Bousquet, P., Poulter, B., Peregon, A., Ciais, P., Canadell, J.G., Dlugokencky, E.J., Etiope, G., Bastviken, D., Houweling, S., Janssens-Maenhout, G., Tubiello, F.N., Castaldi, S., Jackson, R.B., Alexe, M., Arora, V.K., Beerling, D.J., Bergamaschi, P., Blake, D.R., Brailsford, G., Brovkin, V., Bruhwiler, L., Crevoisier, C., Crill, P., Covey, K., Curry, C., Frankenberg, C., Gedney, N., Höglund-Isaksson, L., Ishizawa, M., Ito, A., Joos, F., Kim, H.S., Kleinen, T., Krummel, P., Lamarque, J.F., Langenfelds, R., Locatelli, R., Machida, T., Maksyutov, S., McDonald, K.C., Marshall, J., Melton, J.R., Morino, I., Naik, V., O'Doherty, S., Parmentier, F.J.W., Patra, P.K., Peng, C., Peng, S., Peters, G.P., Pison, I., Prigent, C., Prinn, R., Ramonet, M., Riley, W.J., Saito, M., Santini, M., Schroeder, R., Simpson, I.J., Spahni, R., Steele, P., Takizawa, A., Thornton, B.F., Tian, H., Tohjima, Y., Viovy, N., Voulgarakis, A., Van Weele, M., Van Der Werf, G.R., Weiss, R., Wiedinmyer, C., Wilton, D.J., Wiltshire, A., Worthy, D., Wunch, D., Xu, X., Yoshida, Y., Zhang, B., Zhang, Z., Zhu, Q., 2016. The global methane budget 2000-2012. Earth Syst. Sci. Data 8, 697–751. https://doi.org/10.5194/essd-8-697-2016

Savage, K., Phillips, R., Davidson, E., 2014. High temporal frequency measurements of greenhouse gas emissions from soils. Biogeosciences. https://doi.org/10.5194/bg-11-2709-2014

Semenov, V.M., Kravchenko, I.K., Kuznetsova, T. V., Semenova, N.A., Bykova, S.A., Dulov, L.E., Gal'chenko, V.F., Pardini, G., Gispert, M., Boeckx, P., Van Cleemput, O., 2004. Seasonal Dynamics of Atmospheric Methane Oxidation in Gray Forest Soils. Microbiology 73, 356–362. https://doi.org/10.1023/B:MICI.0000032249.72956.9f

Smith, K.A., Dobbie, K.E., Ball, B.C., Bakken, L.R., Sitaula, B.K., Hansen, S., Brumme, R., Borken, W., Christensen, S., Priemé, A., Fowler, D., Macdonald, J.A., Skiba, U., Klemedtsson, L., Kasimir-Klemedtsson, A., Degórska, A., Orlanski, P., 2000. Oxidation of atmospheric methane in Northern European soils, comparison with other ecosystems, and uncertainties in the global terrestrial sink. Glob. Chang. Biol. https://doi.org/10.1046/j.1365-2486.2000.00356.x

Stielstra, C.M., Lohse, K.A., Chorover, J., McIntosh, J.C., Barron-Gafford, G.A., Perdrial, J.N., Litvak, M., Barnard, H.R., Brooks, P.D., 2015. Climatic and landscape influences on soil moisture are primary determinants of soil carbon fluxes in seasonally snow-covered forest ecosystems. Biogeochemistry. https://doi.org/10.1007/s10533-015-0078-3

Takahashi, M., Hirai, K., Limtong, P., Leaungvutivirog, C., Panuthai, S., Suksawang, S., Anusontpornperm, S., Marod, D., 2011. Topographic variation in heterotrophic and autotrophic soil respiration in a tropical seasonal forest in Thailand. Soil Sci. Plant Nutr. https://doi.org/10.1080/00380768.2011.589363

Tarboton, D.G., 1997. A new method for the determination of flow directions and upslope areas in grid digital elevation models. Water Resour. Res. 33, 309–319. https://doi.org/10.1029/96WR03137

Tonitto, C., Gurwick, N.P., Woodbury, P.B., Del Grosso, S., Ahuja, L., Parton, W., 2016. Quantifying Greenhouse Gas Emissions from Agricultural and Forest Landscapes for Policy Development and Verification, in: Advances in Agricultural Systems Modeling. pp. 229–304. https://doi.org/10.2134/advagricsystmodel6.2013.0007

Vargas, R., Allen, M., 2008. Environmental controls and the influence of vegetation type, fine roots and rhizomorphs on diel and seasonal variation in soil respiration. New Phytol. 179, 460–471. https://doi.org/10.1111/j.1469-8137.2008.02481

Vargas, R., Carbone, M.S., Reichstein, M. and Baldocchi, D.D. 2011 Frontiers and challenges in soil respiration research: from measurements to model-data integration. Biogeochemistry, 102 (1-3), 1-13.

Vargas, R., S. L. Collins, M. L. Thomey, J. E. Johnson, R. F. Brown, D. O. Natvig, and M. T. Friggens. 2012. Precipitation variability and fire influence the temporal dynamics of soil CO_2 efflux in an arid grassland. Global Change Biology 18:1401–1411.

Wang, J.M., Murphy, J.G., Geddes, J.A., Winsborough, C.L., Basiliko, N., Thomas, S.C., 2013. Methane fluxes measured by eddy covariance and static chamber techniques at a temperate forest in central Ontario, Canada. Biogeosciences. https://doi.org/10.5194/bg-10-4371-2013

Warner, D.L., Vargas, R., Seyfferth, A., Inamdar, S., 2018. Transitional slopes act as hotspots of both soil CO_2 emission and CH_4 uptake in a temperate forest landscape. Biogeochemistry 2. https://doi.org/10.1007/s10533-018-0435-0

Warner, D.L., Villarreal, S., McWilliams, K., Inamdar, S., Vargas, R., 2017. Carbon Dioxide and

Methane Fluxes From Tree Stems, Coarse Woody Debris, and Soils in an Upland Temperate Forest. Ecosystems 1–12. https://doi.org/10.1007/s10021-016-0106-8

Webster, K.L., Creed, I.F., Beall, F.D., Bourbonnière, R.A., 2008a. Sensitivity of catchment-aggregated estimates of soil carbon dioxide efflux to topography under different climatic conditions. J. Geophys. Res. Biogeosciences. https://doi.org/10.1029/2008JG000707

Webster, K.L., Creed, I.F., Bourbonnière, R.A., Beall, F.D., 2008b. Controls on the heterogeneity of soil respiration in a tolerant hardwood forest. J. Geophys. Res. Biogeosciences. https://doi.org/10.1029/2008JG000706

Wiesmeier, M., Barthold, F., Blank, B., Kögel-Knabner, I., 2011. Digital mapping of soil organic matter stocks using Random Forest modeling in a semi-arid steppe ecosystem. Plant Soil 340, 7–24. https://doi.org/10.1007/s11104-010-0425-z

Wilson, J., Gallant, J. 2000. Terrain Analysis: Principles and Applications. John Wiley and Sons, New York, NY, USA.

Yvon-Durocher, G., Allen, A.P., Bastviken, D., Conrad, R., Gudasz, C., St-Pierre, A., Thanh-Duc, N., del Giorgio, P.A., 2014. Methane fluxes show consistent temperature dependence across microbial to ecosystem scales. Nature. https://doi.org/10.1038/nature13164